

LA-UR- 00 - 5447

Approved for public release;
distribution is unlimited.

Title:

MAGNETIC IMAGING LENSES FOR
THE ADVANCED HYDRODYNAMIC FACILITY

Author(s):

Andrew J. Jason, LANSCE-1
C. Thomas Mottershead, LANSCE-1
Walter P. Lysenko, LANSCE-1
Filippo Neri, LANSCE-1
Peter L. Walstrom, LANSCE-1
Joseph A. Waynert, ESA-EPE
J. Patrick Kelley, LANSCE-1
John D. Zumbro, P-24
J. H. Schultz, MIT
R. J. Camille, MIT
R. L. Myatt, MIT
A. Radovinsky, MIT
B. Smith, MIT
R. J. Thome, MIT

Submitted to:

2000 ANS/ENS International Meeting
November 13-15, 2000
Washington, D. C.

Los Alamos

NATIONAL LABORATORY

Los Alamos National Laboratory, an affirmative action/equal opportunity employer, is operated by the University of California for the U.S. Department of Energy under contract W-7405-ENG-36. By acceptance of this article, the publisher recognizes that the U.S. Government retains a nonexclusive, royalty-free license to publish or reproduce the published form of this contribution, or to allow others to do so, for U.S. Government purposes. Los Alamos National Laboratory requests that the publisher identify this article as work performed under the auspices of the U.S. Department of Energy. Los Alamos National Laboratory strongly supports academic freedom and a researcher's right to publish; as an institution, however, the Laboratory does not endorse the viewpoint of a publication or guarantee its technical correctness.

DISCLAIMER

This report was prepared as an account of work sponsored by an agency of the United States Government. Neither the United States Government nor any agency thereof, nor any of their employees, make any warranty, express or implied, or assumes any legal liability or responsibility for the accuracy, completeness, or usefulness of any information, apparatus, product, or process disclosed, or represents that its use would not infringe privately owned rights. Reference herein to any specific commercial product, process, or service by trade name, trademark, manufacturer, or otherwise does not necessarily constitute or imply its endorsement, recommendation, or favoring by the United States Government or any agency thereof. The views and opinions of authors expressed herein do not necessarily state or reflect those of the United States Government or any agency thereof.

DISCLAIMER

Portions of this document may be illegible in electronic image products. Images are produced from the best available original document.

MAGNETIC IMAGING LENSES FOR THE ADVANCED HYDRODYNAMIC FACILITY

A. J. Jason, C. T. Mottershead, W. P. Lysenko,
F. Neri, P. L. Walstrom, J. A. Waynert, J. P.
Kelley, and J. D. Zumbro
Los Alamos National Laboratory
Los Alamos, New Mexico 87545
(505) 665 1895

J. H. Schultz, R. J. Camille, R. L. Myatt, A.
Radovinsky, B. Smith, and R. J. Thome
MIT Plasma Science and Fusion Center
17 Albany St., Cambridge, Massachusetts 02139
(617) 253-8100

ABSTRACT

In proton radiography, transmission radiographs of dynamic test objects are made by illuminating the test object with a proton beam from a synchrotron. The energy of the Advanced Hydrodynamic Facility (AHF) synchrotron is 50 GeV. Negative images are formed as denser parts of the test object attenuate the incident beam by nuclear scattering of protons out of the beam more than less-dense parts. However, in addition to the nuclear scattering, smaller-angle multiple Coulomb scattering (MCS) of the protons also occurs in the test object, and introduces a spread in the angles of the protons that are not nuclear-scattered. In proton radiography, this blurring effect is almost eliminated by placing the detector at the focal plane of a point-to-point magnetic quadrupole lens system. A second lens and detector system may be placed downstream of the first system. A third identity lens (the monitor lens) and detector are placed in front of the test object to record the incident beam intensity profile. Because the detectors are thin, a given proton passes through all of the detectors and is detected in all of them with almost unit probability. An additional large-bore quadrupole lens element is placed upstream of the monitor lens and test object to prepare the illuminating beam. In a single three-lens beamline, a total of 13 large-bore quadrupoles is required. In AHF, up to 12 converging and crossing beamlines will be used

to make simultaneous images of the test object over a 180-deg. range of view angles. Improved magnetic-optics performance and larger fields of view can be achieved by use of superconducting quadrupole magnets, which can produce higher pole-tip fields and gradients than conventional quadrupoles. In the paper, the design requirements and operating conditions for the quadrupoles and various approaches to their design are described. Conceptual designs for superconducting quadrupoles of two sizes, based on a NbTi cable-in-channel conductor, are briefly described.

I. MAGNETIC QUADRUPOLE LENS OPTICS

The basic identity lens used in proton radiography¹ is a special quadruplet consisting of two identical cells, as shown in Fig. 1. This lens makes an inverted unit-magnification image of the test object in the image plane. Each cell is a symmetric doublet defined by four parameters—the focal standoff f , the interquad spacer s , and the gradient G and length L of the four quadrupoles. Except for the alternating signs of the gradient, all four quadrupoles are identical. Because of the symmetry, the transfer matrix of this lens shows a remarkable simplicity. If the x -plane transfer matrix of one cell is

$$M \equiv \begin{bmatrix} a & b \\ c & d \end{bmatrix} \quad (1)$$

RECEIVED

DEC 13 2000

OSTI

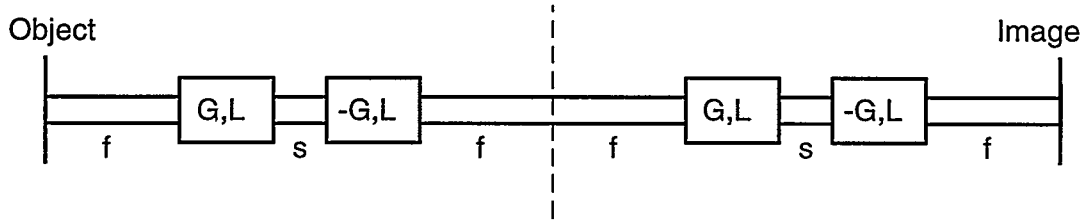


Fig. 1. Configuration of Identity Lens

then that of the two-cell lens is

$$\mathbf{R} = \mathbf{M}^2 = \begin{bmatrix} a\tau - 1 & b\tau \\ c\tau & d\tau - 1 \end{bmatrix} = -\mathbf{I} + \tau\mathbf{M} \quad (2)$$

where $\tau \equiv \text{Tr}(\mathbf{M}) = a + d$ is the trace of the matrix for one cell. To design an identity lens, we need only set the trace $\tau = 0$, leaving $\mathbf{R} = -\mathbf{I}$. (Note that the determinant = 1, always). Similar expressions apply to the y plane. Because of the symmetry, setting the x -plane trace to zero automatically sets the y -plane trace to zero, so only one of the four parameters is consumed in the process. The remaining three parameters remain free to be set by other considerations. In general, the focal standoff f is set by clearance requirements, and the interquad spacer s is set for engineering convenience, e.g. to fit both quads of the doublet in one cryostat. The gradient $G = B_0/(a+g)$ is determined by the quadrupole pole-tip field B_0 , the beam pipe inner radius a , and the radial distance g between the pipe inner radius and the pole-tip radius. For conventional iron-pole-piece electromagnets, a gap of $g=1.5$ cm is reserved between the aperture radius a and the actual iron pole tip. In current-dominated superconducting quadrupoles, the pole-tip radius is defined to be the inner radius of the windings and g is typically 5 cm. In conventional iron-pole-piece electromagnets, B_0 is limited by iron saturation effects to about 1.5 T. Considerably higher pole-tip fields can be achieved with the use of superconducting windings, the value being limited mainly by critical current limits of the superconductor, mechanical stresses, and cost. For a given focal standoff f and pole-tip field B_0 , the aperture radius a , and hence the

quadrupole gradient G are determined by field-of-view requirements. (In this context, field of view refers to the transverse size of the largest object that can be imaged by the lens, with all protons that leave the object with less than a given angular spread passing through the lens system and not striking the inner radius of the beam pipe). The quadrupole length L may then be adjusted to focus the lens for 50 GeV protons. The process must be iterated for a large number of views N (typically $N = 12$), because the width of the quadrupoles depends on a , so the minimum standoff f needed to accommodate N views also depends on a .

All elements of the transport matrix (Eq. 2) are functions of the energy. The lens is in focus (i.e., $R_{12} = 0$) only for the particular proton energy for which $\tau = 0$. The chromatic aberration coefficients, which are the momentum derivatives of the R matrix elements evaluated at the nominal energy, express the fact that at other energies the lens is out of focus and does not have unit magnification. We define $\Delta \equiv \delta p/p$ to be the fractional deviation from the beam momentum for which the lens is in focus and denote the momentum derivatives of the R matrix elements with primes. In order to minimize chromatic effects, we illuminate the object with a correlated (laminar) beam in which the angle of the illuminating rays is a linear function of the distance from the axis, i.e., $\theta = wx$. If w is positive in the x plane, it is equal in magnitude and negative in the y plane. Such a strongly correlated beam appears to come from a (virtual) point source a distance $K = w^{-1}$

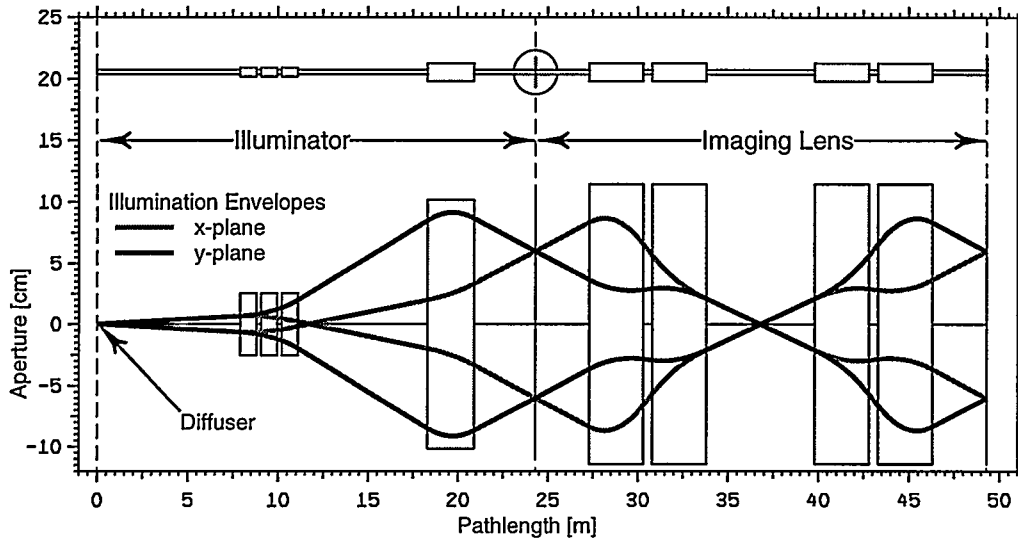


Fig. 2. Schematic of illuminator lens and identity lens system, illustrating preparation of an achromatic illuminating beam. The shaded rectangles represent quadrupole magnets. The radiographed object is placed at the center between the illuminator and imaging lens.

upstream of the lens. The choice $w = -R_{11}' / R_{12}'$ causes $R_{11}' + wR_{12}' = 0$. We call this achromatic correlation because, to first order in Δ , the final position of every proton in the beam that is not scattered from the illuminating ray trajectories is independent of its energy. The mission of the illuminator section in proton radiography is to prepare the incident beam so that only such "achromatic" rays illuminate the object (see Fig. 2). The protons in such an illuminating beam exit the object and enter the lens with trajectory angle $\theta = wx + \phi$, where the scattering angle ϕ represents all deviations from the perfect correlation line due to both incident beam angular spread and scattering in the object. With $R_{12} = -1$, $R_{12}' = 0$ at the nominal proton energy, the final position to lowest order is

$$x_f = -x + C_x \phi \Delta. \quad (3)$$

Here C_x is called the chromatic aberration coefficient of the lens. It is a measure of how much the off-momentum particles are out of focus. Particles with $\Delta = 0$ are in focus, meaning their final position is independent of scattering

angle ϕ . Our aim is to make C_x as small as possible in order to minimize chromatic image blur, with a design goal of 30 meters or less. For example, if $C_x = 30$ meters, particles off momentum by + 0.1%, or $\Delta = 0.001$, or 50 MeV, come to a focus $C_x \Delta = 30$ millimeters past the image plane. Therefore, particles with $\Delta = 0.001$ and an angular deviation of, say, $\phi = 1$ milliradian from the illuminating rays would have an image-plane position shift of 0.03 mm.

Use of the achromatic illuminating rays in this particular lens leads to an additional important behavior that occurs at the midplane of the lens: that of angle sorting. That is, scattered protons with angle of the form $\theta = wx + \phi$ pass through the midplane at a distance x_{mid} from the axis that depends on their scattering angle ϕ , but not on their initial position, as shown in Fig. 3. Then, placement of collimators at the midplane allows cuts to be made on the scattering angle distribution without introducing a large correlation between angle and position. In general, we want the smallest possible focal standoff f to reduce chromatic aberration,

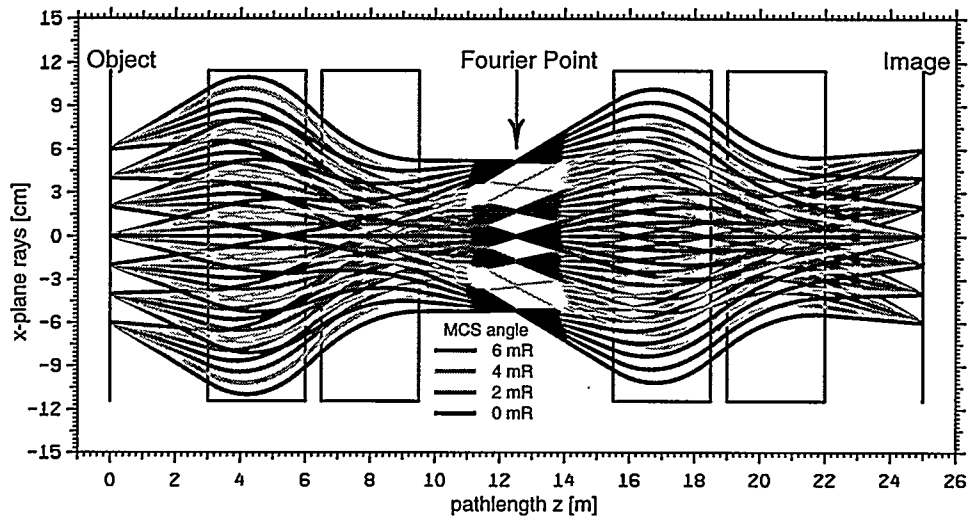


Fig. 3. Illustration of midplane angle sorting with achromatic illuminating rays in the identity lens.

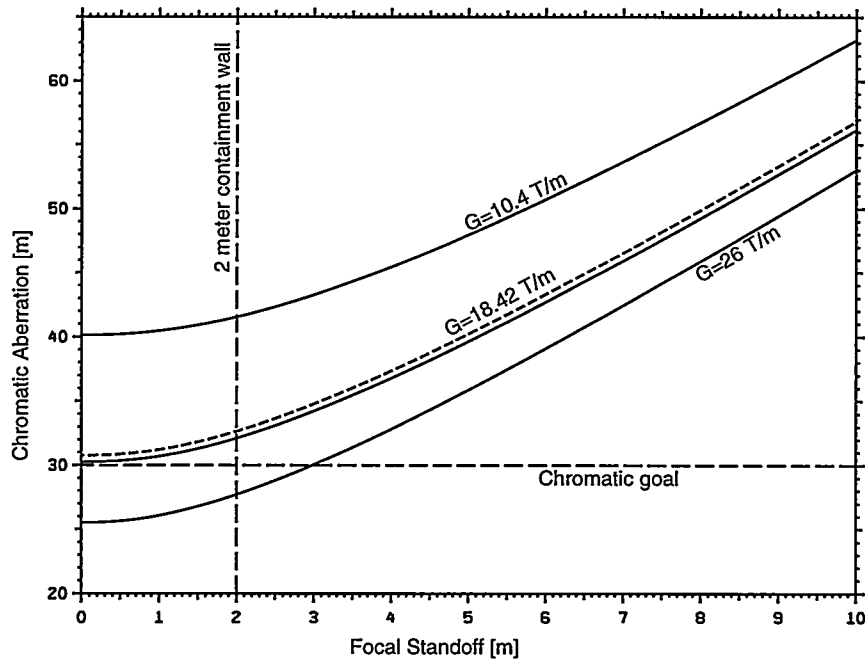


Fig. 4. Dependence of chromatic aberration coefficient C_x on focal standoff f for various gradients.

as well as overall system size. The practical lower limit for f is the larger of the limits given by containment vessel size and mechanical interference between the outer envelopes of quadrupoles in adjacent beamlines. The

presently-used standoff distance of 3 m in AHF studies is determined by interference between quadrupoles. The quadrupole length L needed to focus a lens with given (f,s) depends on the quadrupole gradient G . Figure 4 shows the

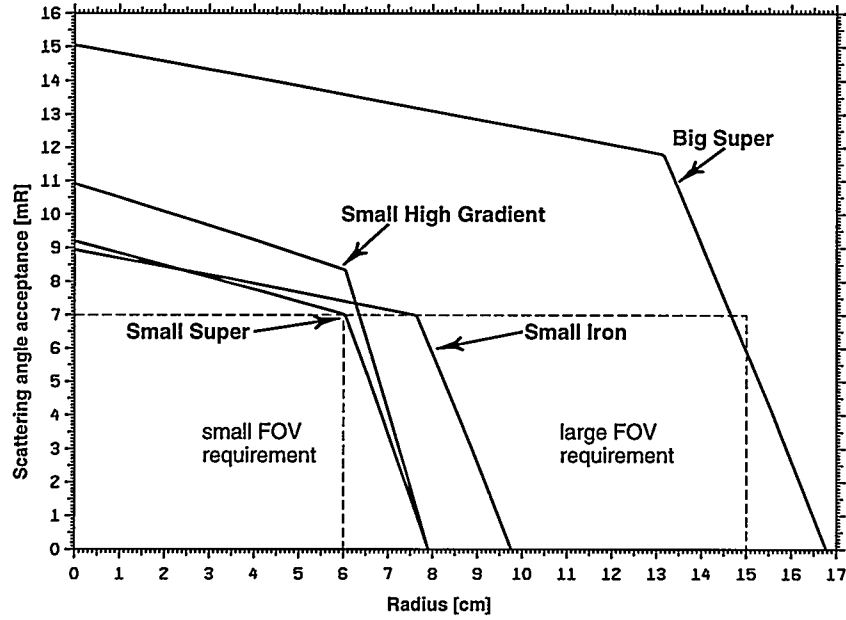


Fig. 5. Field of view for four reference lenses. A given lens passes all protons with object-plane radius and angle that fall below and to the left of the curves. FOV requirements for the two nominal FOV cases are shown by the dashed rectangles.

dependence of chromatic aberration on f for the three reference gradients. The chromatic aberration of a lens depends on its overall length $L_{\text{Tot}} = 4f + 4L + 2s$, and so rises with increasing focal standoff. Note also that higher gradients lead to shorter quadrupoles, and lower chromatic aberration. The solid curves are for $s = 0.5$ m, the dashed curve for $s = 1.0$ m. The chromatic goal of $C_x = 30$ m is met only for the highest gradient, 26 T/m, with $f < 3$ m. Since technical difficulty, cost and outer envelope dimensions for a quadrupole of a given inner bore diameter increase rapidly with gradient, a design with a lower, more realistic gradient (18.4 T/m) and somewhat larger chromatic coefficient (34 m) was chosen for the small-FOV quadrupole in the year 2000 AHF study. A still smaller gradient of 10.4 T/m and larger chromatic coefficient of 43 m were chosen for the large FOV quadrupole. However, because of its larger bore diameter, the lower-gradient large FOV quadrupole has about the same peak winding field as the small FOV quadrupole.

There are two requirement specifications for the field-of-view (see Fig. 5). The small-FOV lens must pass at least 7 milliradians of scattering out to 6 cm off axis. The large FOV lens must pass the same 7 mrad out to 15 cm off axis. The FOV of a lens is determined by the trajectories striking the inside of the beam pipe at the point of maximum excursion and is smaller than the beam-pipe diameter, since the trajectories diverge in some places (see Fig. 4). A rough rule of thumb is that the FOV diameter is about 2/3 of the beam-pipe diameter.

II. THE QUADRUPOLE DESIGN STUDY

In spring-summer 2000 several quadrupole types were studied. Although quadrupoles with the same gradient have the same linear optics, independent of transverse size, large-bore quadrupoles provide a larger FOV but have more geometric aberrations at the outside of the field of view. All lenses in the study were based on a 3-m standoff. The quadrupoles studied included four different 10 T/m quadrupoles with a length

of 4.25 m and a fifth, high-gradient quadrupole magnet, as follows:

1. A room-temperature iron pole-piece conventional quadrupole, pulsed, with a 10-in. ID beam pipe. It was recognized at the outset that conventional magnets of this size could not be used for the full set of 156 magnets in the 12-beamline system because of power-consumption considerations. However, they could have application in single-beamline firing sites, in limited areas where superconducting magnets could not be used, etc.

2. An LN₂-cooled, iron pole-piece conventional quadrupole, pulsed, with a 10 in. ID warm beam pipe. This approach can lower average power consumption, but requires either large reactive power for a short time, or large local capacitive energy storage.

3. A superconducting 10 T/m quadrupole, with a 10-in. ID warm beam pipe, scaled from Jefferson Lab superferric Hall-C Q1 magnet. The scaled magnet has a smaller bore, greater length, the same pole-tip field, yoke and outer cryostat height greater than yoke width (General Atomics scaling and cost study, summer 2000).

4. A superconducting 10 T/m quadrupole, with a 19-in. ID warm beam pipe (the nominal large FOV magnet and Case II of the MIT spring-summer 2000 study).

5. An 18.4 T/m, 9-in. ID warm beam pipe (the nominal small FOV magnet and Case I of the MIT spring-summer 2000 study).

To minimize cryogenic heat loads, two superconducting quadrupoles (a doublet) will be placed inside a single cryostat. The largest effort of the above options was put into Items 4 and 5, the MIT study. The MIT study² included the following design and analysis tasks:

1. A brief survey of applicable winding design and helium cooling approaches- e.g., cable-in-conduit, helium-wetted Rutherford cable, Nb₃Sn vs. NbTi, superfluid bath cooling, etc. and an explanation of the reasons for choosing a particular approach. High current-density magnets are likely to be preferred for reasons of cost.

2. Preconceptual design of the quadrupole for the two cases, including

-Magnetic field analysis, 2-D and 3-D.

-Conductor configuration (dimensions, No. of strands, Cu:S/C ratio, void fraction, I_{op}/I_c , insulation scheme, etc.)

-Winding pack configuration (racetrack coils, cos 2 theta, etc.)

-Structural support scheme- local conductor stresses, radial and tangential forces

-Thermal shields (briefly)

-helium supply manifolds (briefly)

-warm or cold iron yoke, if needed. The feasibility of yokeless designs with correctors was to be investigated by LANL.

-warm beam tube

-availability of space for correctors, if needed (need for and design of to be determined by LANL)

3. Stability analysis

Demonstrate by numerical or/analytic calculations or by scaling from existing magnets that the magnet will achieve design performance. Since only a small portion of one of the 10-14 quadrupoles in a beamline will be subjected to nuclear heating, the magnet cost will be dominated by magnets that can be designed for negligible nuclear heating. Given this basic design, which does not take into account nuclear heating, briefly examine the effect of pulsed nuclear heating, according to data from future hadronic cascade simulations by LANL as available. Preliminary calculations by LANL indicate that this heating can be reduced by shielding to less than 1 millijoule per gram of conductor in the first 10 cm of winding of the first coil downstream of the test object. Heating in the rest of the magnet is smaller and negligible in the rest of the magnets in the lens system.

4. Preliminary stress analysis

- cooldown, Lorentz forces, analysis of local cable stresses

5. Protection scheme and analysis

- maximum hot-spot temperature

- thermal- stress issues

- quench voltages and their relation to the insulation scheme
- 6. Estimate cryogenic system load requirements and specify operating current.
- 7. A cost estimate.

The performance requirements for the quadrupoles of the MIT study are listed in the following table.

Table I. Performance requirements for MIT Cases 1 and 2.

Parameter	Case I	Case II
FOV (6 mrad)	14 cm	30 cm
Beam-Pipe ID	9 in.	19 in.
Warm-bore ID	11 in.	21 in.
Central Gradient	18.4 T/m	10.4 T/m
Magnetic length (one quadrupole)	2.90 m	4.25 m
Integral gradient (one quadrupole in doublet)	53.6T	43.8 T

It was assumed that the beam pipe would be an independently supported inner pipe connected to the containment vessel. The quadrupole doublet cryostat will have a warm bore with an inner diameter larger than the outer diameter of the beam pipe to provide for a radial gap to accommodate movement of the beam pipe during dynamic experiments. Supports for the beam pipe will be designed to minimize mechanical coupling between the beam pipe and the superconducting magnets and cryostat. A radial gap of between 0.25 in. to 0.5 in. between the two was assumed in this study.

The nominal pole-tip field (field at the inner winding radius computed as the product of the central gradient and the winding inner radius) for the Case-I magnets is 3.3 T. The peak winding field is 4.9 T. For the Case I magnets of the study MIT chose to use for the conductor the SSC NbTi dipole cable. Sufficient quantities of this cable exist for use in prototype development. In the conductor for the MIT study, the cable is

to be soldered into a copper channel. This concept provides both greater radial strength for an edge-wound conductor and additional stability for quench recovery. The cable in copper in channel operates at 4.3 K and the windings are cooled with two-phase helium. The windings are two-layer windings of the cos 2θ type and are yokeless and collared with precompression.

The study examined designs with and without epoxy impregnation from the point of view of mechanical strength and stability against thermal loads. Stress analysis indicated that the potted winding pack concept together with an external collar with precompression was a credible mechanical design approach and met all stress allowables for the materials.

Although the design was based on a yokeless concept in order to minimize interference between magnets nearest the firing point, addition of a warm iron shield or yoke outside of the cryostat where space permits is feasible. Use of a shield or yoke with a circular ID as in typical accelerator ring magnets adds relatively little to the quadrupole gradient (relatively more with low-field magnets, less with high-field magnets if saturation is minimized), but is desirable for field-quality reasons. Iron yokes or shields would have a circular inner diameter and an outside shape that would be rectangular where space is limited and circular where available space is greater. The shield will be used wherever possible to reduce coupling (both of magnetic field errors and magnetic loads) between adjacent beamlines and nearby ferromagnetic structures. Since we may want to use our lenses at reduced beam energy (say 25 GeV), use of superferric magnets with highly saturated iron undesirable.

The MIT magnets as designed can be protected from quench damage by use of an external energy dump with up to four quadrupoles in series.

In stability calculations, the largest expected heat input in the windings is pulsed nuclear heating by particles scattered from and produced

in the test object. This has a significant effect only on those magnets immediately downstream of the test object. Recent MCNP-X results for the small, high-gradient superconducting lens quadrupole (Lysenko) show that without shielding at the inner radius of the magnet, peak energy deposition (2×10^{12} protons) will be about 0.35 mJ/g, which leads to a temperature rise of about 2 K. Designing for this relatively large heat input is possible, but it requires relatively expensive designs (use of niobium tin superconductor instead of NbTi superconductor, etc.). Adding one inch of tungsten at the inner bore of the magnet plus shielding at the end reduces the peak and average heating by a factor of approximately four. With the shield, the design has enough margin in operating current over critical current (I_{op}/I_c) that the conductor temperature T reached just after beam pulses as computed by nuclear heating codes never exceeds the current-sharing temperature T_{cs} . Since the heating results came too late in the study to be incorporated into the final MIT design, the magnet size studied is based on the magnets without the shield. However, the unshielded magnets constitute 12 of the 13 large-bore magnets in a beamline. Therefore, the net cost impact of nuclear shielding on the overall lens system is expected to be small, but for the shielded magnets, the resultant increase in winding radius will presumably cause increase in peak winding field, stresses, and cryostat OD.

We may need to revisit the nuclear-heating results for the large-bore S/C magnet (MIT Case II), since the earlier calculations for this larger magnet did not emphasize finite-object-size effects in computing nuclear heating.

A study of field-quality issues was begun at LANL in the summer 200 study, but more work remains to be done. Preliminary tracking results indicate that a two-part specification is required. The field errors are specified at ID of beam pipe. The two-part specification includes a central-field error specification and an end-field error specification:

1. Central field: sum of absolute values of all error Fourier components to be no more than 0.001 of the quadrupole component.

2. End-field: sum of absolute values of all error Fourier components, integrated through a single end region, to be no more than 0.001 of the GL product of the quadrupole.

These requirements can be met either by the quadrupole alone or by a quadrupole plus a system of correctors. The present MIT designs do not meet the end-field requirement (solving field-quality issues was not part of the MIT statement of work). It should also be noted that use of correctors may be cheaper than refining the quadrupole design with special end-turn shaping and spacing. Correctors may be needed in any case to correct geometrical aberrations and certainly will be needed to correct stray-field effects from yokeless quadrupoles in adjacent beamlines, if yokeless quadrupoles must be used to minimize mechanical interference. This is another subject for future study.

III. CONCLUSIONS

The basic quadrupole magnetic-optics concepts and requirements and design goals for proton radiography at 50 GeV in an AHF have been described. Cost-effective conceptual designs of superconducting quadrupoles that meet the basic AHF requirements have been demonstrated.

REFERENCES

1. C. T. Mottershead and J. D. Zumbro, "Magnetic Optics for Proton Radiography", proc. 1997 Particle Accelerator Conference, Vancouver, B.C., May 1997, p. 1397 (IEEE Pub. 9CH36167).
2. J. H. Schultz, R. J. Camille, C. Y. Gung, A. Radivinsky, B. Smith, R. J. Thome, J. V. Minervini, R. L. Myatt, P. L. Walstrom, and J. A. Waynert, "Superconducting Quadrupoles for Proton Radiography in the Advanced Hydrodynamics Facility", paper presented at the Applied Superconductivity Conference, Virginia Beach, Virginia, Sept. 17-22, 2000.